Review of Scientific Instruments

RESEARCH ARTICLE | FEBRUARY 14 2022

A non-motorized spectro-goniometric system to measure the bi-directional reflectance spectra of particulate surfaces in the visible and near-infrared

Te Jiang ; Hao Zhang ; Yazhou Yang ; Pei Ma ; Yuxue Sun; Yan Zhuang

Rev. Sci. Instrum. 93, 024504 (2022)
https://doi.org/10.1063/5.0071621

AIP Publishing

Review of Scientific Instruments ARTICLE scitation.org/journal/rsi

A non-motorized spectro-goniometric system to measure the bi-directional reflectance spectra of particulate surfaces in the visible and near-infrared

Cite as: Rev. Sci. Instrum. 93, 024504 (2022); doi: 10.1063/5.0071621
Submitted: 15 September 2021 • Accepted: 26 January 2022 •
Published Online: 14 February 2022

Te Jiang,[1] Hao Zhang,[1,2,a)] Yazhou Yang,[3] Pei Ma,[1] Yuxue Sun,[1] and Yan Zhuang[1]

AFFILIATIONS

[1] Planetary Science Institute, School of Earth Sciences, China University of Geosciences, Wuhan, China
[2] CAS Center for Excellence in Comparative Planetology, Hefei, China
[3] State Key Laboratory of Space Weather, National Space Science Center, Chinese Academy of Sciences, Beijing, China

[a)] **Author to whom correspondence should be addressed:** zhanghao@cug.edu.cn

ABSTRACT

Reflectance spectroscopy is a powerful tool for remotely identifying the compositional and physical properties of surface materials. Due to the anisotropic scattering nature of most surfaces, the spectral features, including the absolute reflectance value, spectral slope, and band depth, are influenced by illumination and viewing configurations. Therefore, it is important to understand how spectral features vary with illumination and observation geometries for various particulate surfaces through laboratory measurements. Here, we describe a non-motorized spectro-goniometric system capable of measuring the bi-directional reflectance of particulate surfaces in the upper hemisphere in the wavelength range from 350 to 2150 nm. The incident and the viewing zenith angles can be varied from 0° to 55° and from 0° to 70°, respectively. The relative viewing azimuth angle can be varied from 0° to 360°. Measurements on Labsphere Spectralon agree well with measurements done with other instruments. We also present measurement results on two typical planetary analog materials, the JSC-1A Martian soil simulant and the JSC-1A lunar regolith simulant.

I. INTRODUCTION

Reflectance spectroscopy has been widely used in the Earth and planetary remote sensing to retrieve the compositional and physical information of surficial materials (e.g., Hapke, 2012). However, the quantitative interpretations of reflectance spectra made at arbitrary scattering configurations are not always straightforward, as the spectral reflectance value, spectral slope, and absorption band depth of many natural surfaces would depend on illumination and viewing geometries; for example, as the solar phase angle (the angle between the incident and the viewing directions) changes, the surfaces of many solid bodies and laboratory analog materials exhibit varied spectral slope (e.g., Gehrels *et al.*, 1964; Adams and Filice, 1967; Guinness, 1981; Abe *et al.*, 2006; Johnson *et al.*, 2013; Schröder *et al.*, 2014, and Clark *et al.*, 2002) and absorption band depths (e.g., Veverka *et al.*, 1978a; 1978b; and Hapke; 2012). Conversely, most laboratory reflectance measurements are performed at limited scattering geometries; for example, the library spectra of NASA's Reflectance Laboratory (RELAB) are mostly measured at $i = 30°$, $e = 0°$, and $\alpha = 30°$, where i, e, and α are the incident zenith, viewing zenith, and solar phase angles, respectively (Pieters and Hiroi, 2004). To compare with library spectra, it is common practice to perform photometric corrections to transform remote sensing spectra measured at the arbitrary geometry to the standard laboratory geometry. Therefore, the accurate interpretations of remote sensing spectra would rely on a thorough understanding of the multi-angular reflectance behavior of various samples.

The design trade-offs of laboratory spectro-goniometers that can make multi-angular reflectance spectral measurements include

a number of factors, such as the spectral coverage, the incident and the viewing angular ranges and angular resolutions, polarization capabilities, level of automation, cost, and many others. Although motorized systems are becoming increasingly popular for modern goniometers (e.g., Shepard, 2001; Pieters and Hiroi, 2004; Gunderson *et al.*, 2006; 2007; Shepard and Helfenstein, 2007; Shkuratov *et al.*, 2007; Sun *et al.*, 2014; and Pommerol *et al.*, 2019), the presence of motorized moving parts would increase system complexity and construction cost and thus, sometimes, a manual design may be preferred. Here, we describe a non-motorized and cost-effective bi-directional reflectance spectro-goniometer system capable of measuring the spectral reflectance of particulate layers from 350 to 2150 nm. Detailed descriptions of the instrument are given in Sec. II. The calibration and validation results are presented in Sec. III, and planetary analog measurement results are given in Sec. IV.

II. INSTRUMENT DESCRIPTION AND SAMPLE PREPARATION

Figure 1 shows the spectro-goniometric system that consists of three major parts: the light source, a goniometer, and a spectrometer. The incident zenith angle i, the viewing zenith angle e, the phase angle α, and the relative azimuth angle ϕ are illustrated in Fig. 2. Detailed descriptions of the system are as follows.

A. Light source and illumination optics

We use a highly stable Newport 66502-250Q-R1 Quartz Tungsten Halogen (QTH) light source as the incident light for the system [Fig. 1(c)]. The QTH lamp (model number 6334NS) has a maximum flux of ~10 000 Lumens and a 3400 K color temperature. The output irradiance curve of the QTH light source can be found at https://www.newport.com/f/qth-lamps, and the output power of the lamp is adjustable from 0 to 250 W. Light from the bulb is first collimated by a concave mirror and is then inserted into a Newport 77576 fiber optic cable by a Newport 77776 Focusing Assembly. The 91-cm-long fiber optic cable used for illumination has a numerical aperture of 0.22 and can transmit light in the wavelength range of 260–2200 nm. The spectral transmittance of this fiber is mostly around 50% except across the two absorption regions around 1200 nm (~40%) and 1400 nm (~5%) (https://www.newport.com/p/77576). A Newport 77646 collimator (https://www.newport.com/p/77646) is mounted at the other end of the fiber to collimate the incident beam and adjust the incident spot size.

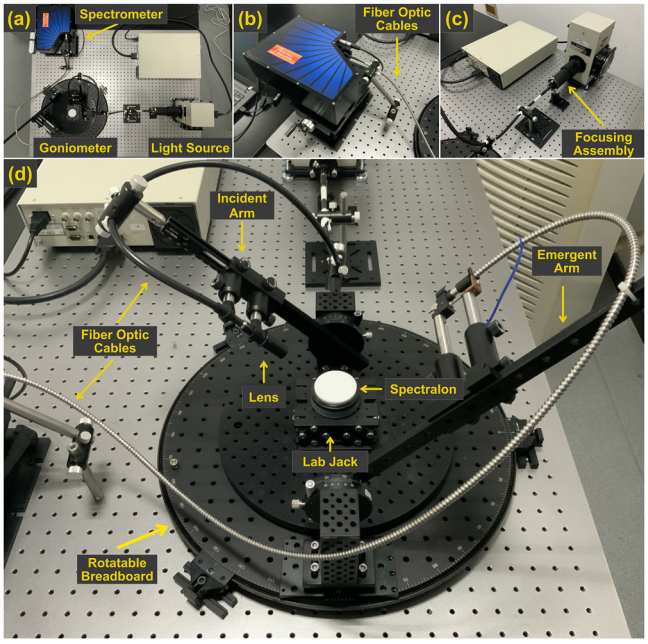

FIG. 1. The spectro-goniometer system: (a) overall layout, (b) the spectral evolution SR-2500 spectrometer, (c) the quartz tungsten halogen light source, and (d) a closer view of the goniometer.

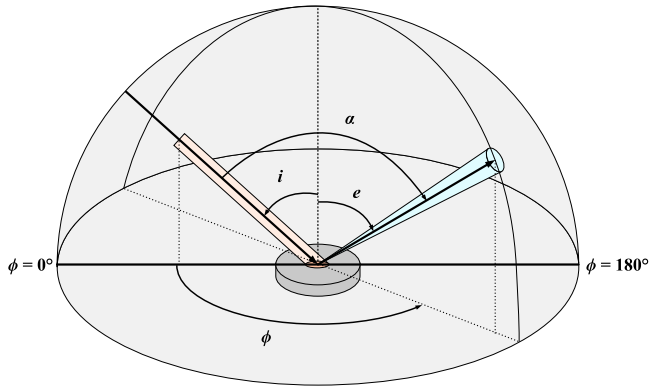

FIG. 2. Schematics of the reflectance geometry. A collimated beam is incident onto the surface from the incident zenith angle i and the azimuth angle $\phi = 0°$. The reflected radiance is viewed from the viewing zenith angle e and the relative azimuth angle ϕ. The phase angle α is the angle between the incident and the viewing directions. e and ϕ vary between 0°–90° and 0°–360°, respectively. For scattering in the principal plane (the plane containing the incident, surface normal, and viewing directions), backward and forward scattering directions are designated with positive and negative e values, respectively.

B. The goniometer

The goniometer part of the system [Fig. 1(d)] includes a 30-cm-long incident optics arm and a 60-cm-long viewing optics arm, both mounted on rotary stages (Edmund Optics 66516) that are connected to mounting blocks (Thorlabs part No. TS240 "tombstone"), which are, in turn, installed on a large rotatable breadboard. Both the incident and the viewing arms can be manually adjusted from 0° to 90°. However, due to the elongation of the incident light spot and the lower collection efficiency at large zenith angles, in most measurements, the maximum incident and the viewing zenith angles have been limited to 55° and 70°, respectively. The relative azimuth angle ϕ between the incident and the viewing directions is adjustable from 0° to 360°. The vernier scales of the rotational breadboards (Fig. 3) allow zenith and azimuth precisions of 10′ (1/6°) and 5′ (1/12°), respectively. Due to the mechanical interference between the incident and the viewing arms, angular positions near the opposition

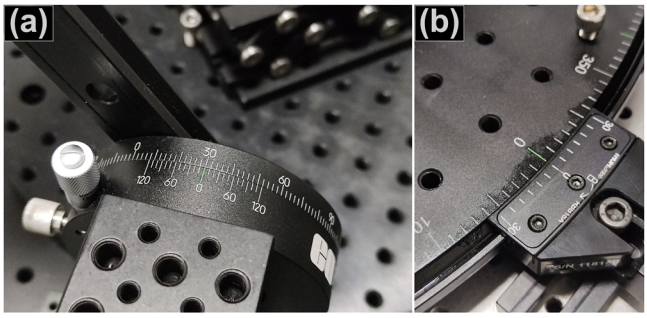

FIG. 3. A closer view of the rotatable breadboards for zenith (a) and azimuth (b) angular directions with angular resolutions of 10′ (1/6°) and 5′ (1/12°), respectively.

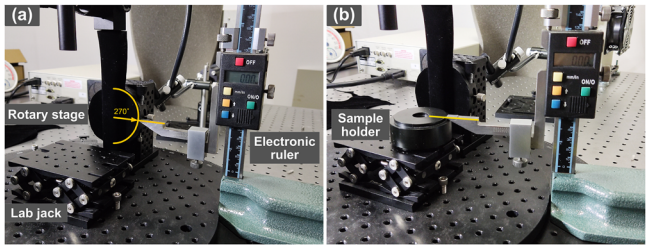

FIG. 4. By using an electronic ruler with a precision of 0.01 mm, the center of the incident/viewing bar rotary stage (a) can be easily leveled with the surface of the sample holder mounted on a lab jack (b).

($\alpha < 10^\circ$) and some angular positions with ϕ between 270° and 360° are not attainable.

The sample holder is placed on a lab jack mounted on the rotary breadboard so the sample can be easily raised and lowered. By using an electronic ruler with a precision of 0.01 mm, the sample surface is easily leveled with the centers of the incident and the viewing rotary stages, as shown in Fig. 4. The tilting of different surfaces in the goniometric system is checked by a digital protractor with a precision of 0.05°, and the typical results are summarized in Table I. Obviously, the surfaces of various components are aligned with each other very well.

The collimator for the incident fiber is installed on the incident arm and is placed ~8 cm above the sample surface. At normal incidence, the incident collimator forms a circular spot with ~1.5 cm diameter on the sample surface. As the incident zenith increases, the spot becomes an elongated oval with a maximum length of 2.6 cm at 55° incidence. The scattered light is collected by a 1.2-m-long optical fiber with its tip placed 15 cm away from the sample surface. The fiber has a numerical aperture of 0.42 and views a ~14-cm-diameter circular spot, which is much larger than the diameter of the sample holder (3.5 cm diameter). In other words, we have adopted an "over-view" scheme that can effectively improve the signal-to-noise ratio (SNR) (e.g., Voss *et al.*, 2000 and Zhang and Voss, 2008). This option was selected based on the following discussion.

As shown in Fig. 5, when the field of view is commensurate with the incident spot size (in brown), the viewed area (in light blue) can be larger or smaller than the incident spot during a measurement. Specifically, if the measurement is performed in the principal plane, the viewed area is generally smaller than the illumination spot when $i > e$ [Fig. 5(a)]; when $i < e$, the opposite is true [Fig. 5(b)]. When the measurement is performed outside of the principal plane [Fig. 5(c)], things get more complicated as the viewing optics can only see part of the illuminated spot. As a result, the measured angular scattering behavior of the surface may be distorted.

For these reasons, people usually stay with either the over-illumination or the over-view scheme to make sure the measured angular scattering behavior stays consistent during the measurement. Although the over-view scheme has the disadvantage that the detected radiance from a Lambertian-type surface decreases as the cosine of the viewing zenith angle due to a smaller fraction of viewed area at a larger viewing zenith angle, it has several advantages over the over-illumination scheme. First, over-viewing the illuminated area improves the collection efficiency and makes the sensor alignment less critical. Second, if the illuminated area has a non-uniform structure, viewing only a portion of the light spot would cause large errors. Therefore, we have adopted the over-view design for our instrument.

Although the collected area is much larger than the sample holder area, the largest diameter of the incident beam is

TABLE I. A typical measurement of the tilting angles of the different surfaces of the goniometric system. The angles were measured by a digital protractor with a precision of 0.05°. Positive and negative angles correspond to counter-clockwise and clockwise tilting when the observer is facing the system [see Fig. 14(a) below].

Photo of the goniometer	Surface	Tilting angle (deg)	
		North–south	East–west
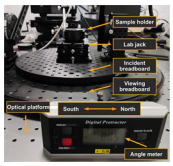	Sample holder	+0.05	−0.10
	Lab jack	+0.05	−0.10
	Incident breadboard	0.00	−0.10
	Viewing breadboard	0.00	−0.10
	Optical platform	+0.05	−0.10

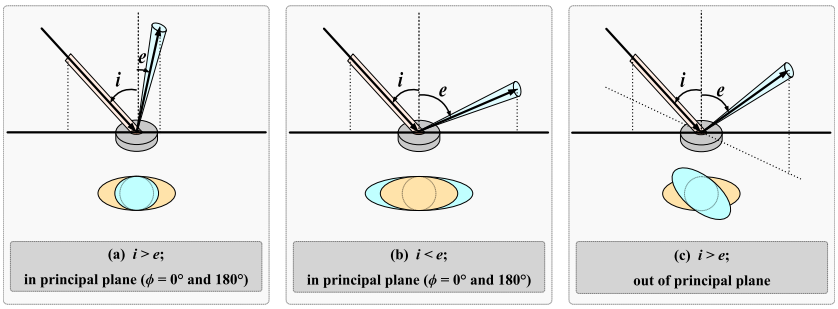

FIG. 5. Comparisons of the incident (brown) and the viewing (light blue) areas in different scattering configurations. (a) $i > e$, in the principal plane, (b) $i < e$, in the principal plane, and (c) $i > e$, outside of the principal plane.

2.6 cm (at 55° incidence), which is much smaller than the diameter of the sample (3.5 cm), and thus no direct illumination is incident on the non-sample parts. The secondary and higher-order reflections from non-sample parts are suppressed by covering some of the reflective metallic parts using black velvets sprayed with a water-based acrylic paint, Musou Black (https://www.ko-pro.black/product/musou-black-paint/), which is one of the blackest commercially available black paints. With these measures, reflections from non-sample parts have a negligible effect on the viewed signal.

C. The spectrometer

The spectrometer is a Spectral Evolution SR-2500 spectrometer [Fig. 1(b)] that covers the spectral range from 350 to 2500 nm and has spectral resolutions 5 nm at 350–1000 nm and 22 nm at 1500–2100 nm, respectively (https://spectralevolution.com/products/hardware/compact-lab-spectroradiometers/sr-2500/). Its detectors include a 512-element UV-enhanced silicone array in 350–1000 nm and a 256-element thermal electrically cooled extended InGaAs array in the 1000–2500 nm region. The number of averages is selectable from 1 to 100 and the typical noise equivalence radiances with a 1.2-m-long optic fiber are $0.8 \cdot 10^{-9}$ at 400 nm, $1.5 \cdot 10^{-9}$ at 1500 nm, and $1.8 \cdot 10^{-9}$ at 2100 nm, all in W/cm^2/nm/sr. Data in ASCII format are acquired through the DARWin SP Data Acquisition software in Windows 7 operating system.

D. Sample preparations

We use the JSC-1A Martian Soil Simulant (JSC-1A MSS) acquired from Orbitech to demonstrate how a measurement surface is made. As illustrated in Fig. 6, we first slowly scooped powdery grains into the sample holder with a spoon and then moved the edge of a straight knife along different directions to smooth the surface. Since we want to equalize the porosities of various granular samples, we did not compress the sample by any means. After cleaning up the grains scattered on the sample holder edge, we covered the sample holder with a circular-ring-shaped black velvet to reduce any possible reflections from the sample holder [Fig. 6(f)].

III. CHARACTERIZATIONS AND CALIBRATIONS

In this section, we first present the test results on noise, linearity, and stability. Then, we describe the data reduction methods and compare our Spectralon measurement results with the published ones.

A. Noise and stray light evaluations

For the goniometric system placed in a dark room, three major types of noise may affect measurement results: stray light in the darkroom, electrical noise from the spectrometer circuits, and spurious light signals produced by multiple reflections of light off various optical components. The contributions of these noises and stray light on measurement can be estimated as follows: (1) we first make a measurement on Spectralon with the light source off and the viewing fiber blocked by a plastic block to get the electrical noise; (2) next, we remove the block and turn on a table lamp placed near the goniometer and make another measurement to include both the electrical and the background noises; (3) then, we turn on the light source (output power set at 200 W), block the viewing fiber, and make the third measurement, which includes all three types of noises; (4) a normal measurement on Spectralon with 99% nominal reflectance with the

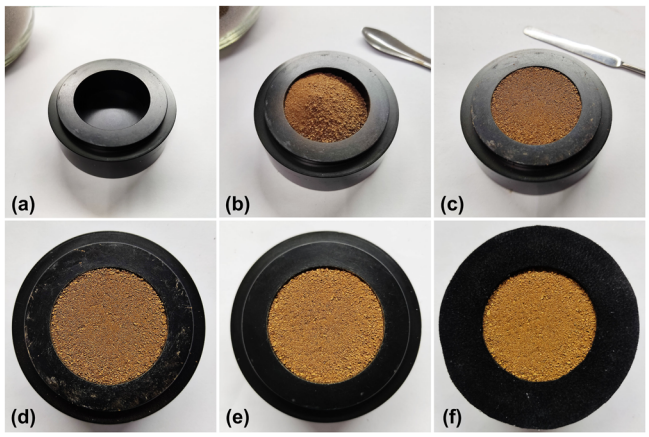

FIG. 6. A typical sample preparation process demonstrated with the JSC-1A MSS: (a) The empty sample holder, (b) powdery grains loaded into the sample holder, (c) the surface smoothed by moving the edge of a straight knife, (d) top view of (c), (e) with particles scattered on the edge of the sample holder removed, and (f) the sample holder edge covered by a circular-ring-shaped black velvet to reduce stray light.

light source on (output power set at 200 W), the table lamp off, and the viewing fiber block removed was carried out; and (5) same as (4), but the sample is changed to a very dark volcanic sand collected from the Big Island, HI.

The results of measurements (1)–(5) are shown in Fig. 7(a), and the effect of averaging repeated measurements for the very dark volcanic sand is shown in Fig. 7(b). Test 1 shows that the system electrical noise is on the level of ~0.01% in the visible and less than 0.5% above 1 μm except at the connecting region of the two detectors (~0.9 μm). Test 2 is to simulate the situation when the operator forgets to turn off the lamp during a measurement, an extreme case of strong ambient light. It turns out the lamplight only strongly affects the visible part of the spectrum and its spectrum can be easily identified from the measured spectrum [Fig. 7(a)]. If this occurs, we can redo the measurement with the lamp off. Test 3 includes both the electrical noise and the ambient light contribution, and the measured signal is not significantly different from the result of Test 1. This demonstrates that the ambient noise is negligible. Test 4 includes the electrical noise, the ambient light, and the stray light from higher-order reflections from non-sample parts of the system. Obviously, the stray light contribution is also negligibly small. In measurement 5, the signal-to-noise ratio is still very good (better than 1%) in the visible region, but the noise dominates the near-infrared (NIR) region. Therefore, we need repeated measurements to reduce the noise level for dark samples. As shown in Fig. 7(b), the noise level can be reduced to ~5% after an average of 100 measurements.

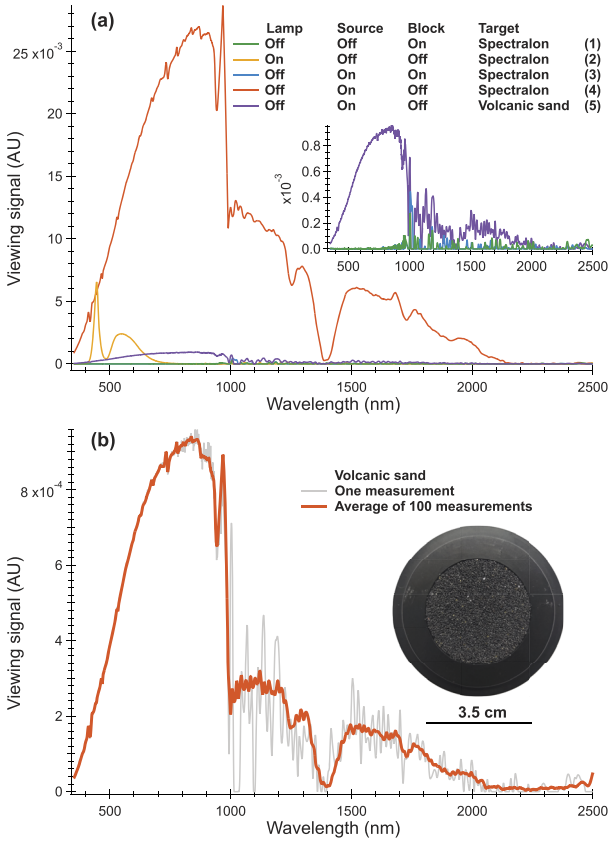

FIG. 7. Estimation of the three kinds of noise. AU stands for an arbitrary unit. Measurements (1)–(5) are described in the text.

B. Linearity

The linearity performance of the system was tested by setting the light source at five different power levels, 25, 50, 100, 150, 200, and 225 W and measuring the signal values from Spectralon at a fixed configuration of the incident zenith 30° and the viewing zenith 0° in the principal plane. During the measurement, we fixed the integration time and the number of measurements. We sequentially placed nine laser line/bandpass filters (Fig. 8) between the incident collimator and the sample to measure the power using a power meter and then used the spectrometer to measure the light reflected from Spectralon. Figure 9 shows the averaged viewing signal values vs incident power, suggesting that the system has good linearity.

C. Stability

The stability test was performed under a fixed geometry of the incident zenith 45° and the viewing zenith 0° in the principal plane. We measured the viewing signal values of the Spectralon surface every 1 min within 0.5 h, and each of the 31 measurement spectra was divided by the first measurement to obtain the relative fluctuations. Figure 12 shows the 31 individual measurements [Fig. 10(a)] and the ratios [Fig. 10(b)] with their averages. If the system is perfectly stable, the ratios should be a 100% horizontal line. As shown in Fig. 10, the system is highly stable in 350–960 nm with ~0.5% fluctuations and moderately stable in 960–2150 nm with ~4% fluctuations, except for the noisier data around 1400 nm and beyond 2000 nm caused by the absorption features of the incident optic fiber and the water vapor at ambient conditions at these wavelengths. However, the fluctuations in 960–2150 nm can be significantly reduced to about 0.5% by averaging multiple measurements.

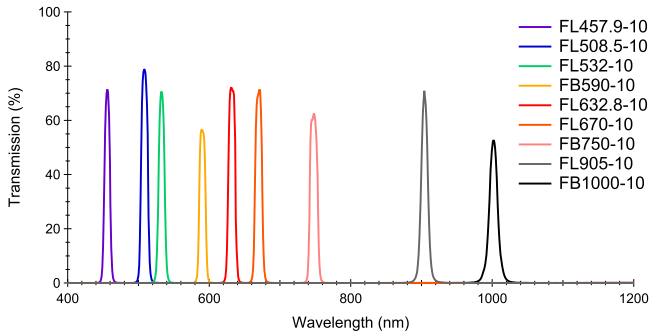

FIG. 8. Transmission curves of the filters used in the linearity test. FL and FB stand for laser line and bandpass filters, respectively, followed by the center wavelength in nm. The number after the dashed line is the full width at half maximum (FWHM) of the filter. In this work, all filters have an FWHM of 10 nm.

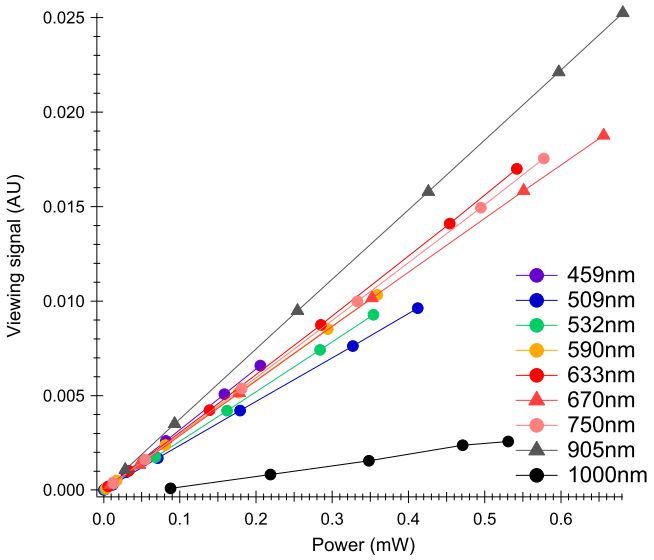

FIG. 9. Linearity test of the spectro-goniometer. The power of the light source was set at 25, 50, 100, 150, 200, and 225 W. The power (horizontal axis) was measured by an optical power meter with its sensor placed between the incident collimator and the sample surface, and the viewing signal reflected from Spectralon (vertical axis) was measured by the spectrometer. The incident and the viewing zenith angles were fixed at $i = 30°$ and $e = 0°$ in the principal plane, and the number of averages was set to be 30. The wavelengths were selected based on the center wavelengths of the filter shown in Fig. 8. Since the spectrometer automatically interpolates the output data to have a 1 nm interval, any wavelength values with fractions were rounded to integers (e.g., the wavelength of the FL632.8–10 filter was rounded to be 633 nm). The vertical axis is in arbitrary units (AU).

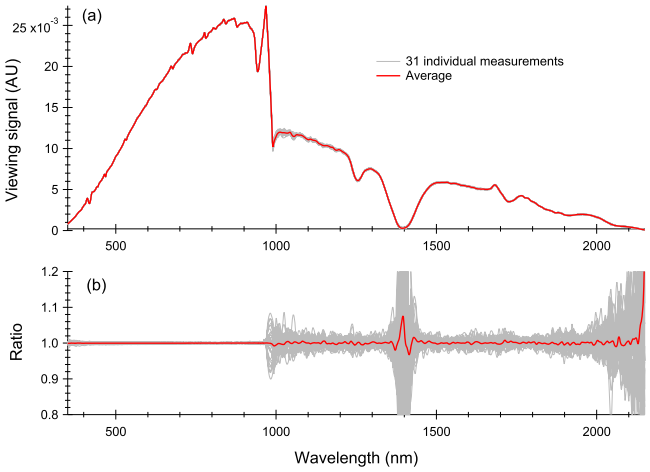

FIG. 10. Stability test results of the spectro-goniometer. (a) Original signals of the 31 measurements and (b) ratios of all measurements to the first. The vertical axis of (a) is in arbitrary units (AU).

D. Data reduction and comparisons with previous measurements

We use a Labsphere Spectralon with 99% nominal reflectance both as the calibration target and the standard sample to characterize the scattering behavior of our spectro-goniometer. We present the reflectance data in terms of the reflectance factor (*REFF*), which is defined as the ratio of the bi-directional reflectance of the sample to that of a perfectly diffuse surface under the same geometry of illumination and measurement (Hapke, 2012). We first obtain the relative reflectance $R_r(i, e, \phi, \lambda)$ as

$$R_r(i,e,\phi,\lambda) = \frac{I_{sample}(i,e,\phi,\lambda)}{I_{spectralon}(i,e,\phi,\lambda)}, \quad (1)$$

where $I_{sample}\ (i, e, \phi, \lambda)$ and $I_{spectralon}\ (i, e, \phi, \lambda)$ are the radiance from the sample and Spectralon measured at the incident zenith i, the viewing zenith e, the relative azimuth angle ϕ, and the wavelength λ. Since the viewing signal of our radiometer is proportional to radiance, we can replace the absolute radiance in Eq. (1) with the viewing signal values. The sample *REFF* can then be obtained as (Zhang and Voss, 2005 and Voss and Zhang, 2006)

$$REFF_{sample}(i,e,\phi,\lambda) = R_r(i,e,\phi,\lambda) REFF_{Spectralon}(i,e,\phi,\lambda), \quad (2)$$

where $REFF_{Spectralon}(i, e, \phi, \lambda)$ is the *REFF* of Spectralon obtained from the absolute measurement.

The $REFF_{Spectralon}$ has been measured by many groups (e.g., McGuckin *et al.*, 1996; 1997; Bruegge *et al.*, 2001; Bhandari *et al.*, 2011; and Svensen *et al.*, 2012) and the data provided by NASA's Multi-angle Imaging Spectro Radiometer (MISR) team (McGuckin *et al.*, 1996; 1997 and Bruegge *et al.*, 2001) are one of the most widely used. The MISR Spectralon data were collected at three wavelengths (442, 633, and 866 nm) and at five discrete incident zenith angles, 8°, 40°, 45°, 50°, and 55°, various viewing zenith angles from 1° to 80°, and relative azimuth angles from 0° to 180°. In order to use the MISR $REFF_{Spectralon}$ to calibrate our data using Eq. (2), we used the same incident zenith angles in our measurements. However, we limited our viewing zenith angle to be smaller than 70°, as, at very large viewing zenith angles, the radiometer has very low collection efficiencies. The $REFF_{Spectralon}$ needed in Eq. (2) is obtained by using Eq. (3) below as (using 633 nm as an example)

$$REFF_{Spectralon}(i,e,\phi,633\text{ nm}) = \frac{I_{spectralon}(i,e,\phi,633\text{ nm})}{Cos(e)} A, \quad (3)$$

where A is a correction factor at a specific viewing position (here $e = 1°$ and $\phi = 0°$) that normalizes our measurement data to that of the MISR *REFF*, $REFF^{MISR}_{Spectralon}$, and then, the *REFF* of the sample at 633 nm can be obtained using Eq. (2). We used different A's for different incident angles, but their relative differences are less than 1%. Since the MISR $REFF^{MISR}_{Spectralon}$ in three wavelengths (442, 633, 866 nm) have nearly identical photometric properties (viewing zenith angular dependence) (Bruegge *et al.*, 2001), we assumed that the Spectralon has similar photometric behavior in the visible and near-infrared regions, and this assumption allowed us to scale our *REFF* data to MISR's data through one simple constant at 633 nm (Yang *et al.*, 2019). It should be noted that, although we used a normalization constant [A in Eq. (3)] to scale our measurement to

the MISR *REFF*, such normalization would not change the angular behavior of our measured data.

Finally, the Spectralon spectrum measured by RELAB (Yang *et al.*, 2019), $REFF^{RELAB}_{Spectralon}(i = 30^\circ,\ e = 0^\circ,\ \phi = 0^\circ,\ \lambda)$, is used to calibrate the wavelength dependence of the Spectralon reflectance as

$$REFF_{spectralon}(i, e, \phi, \lambda) = REFF_{Spectralon}(i, e, \phi, 633\ \text{nm}) * REFF^{RELAB}_{Spectralon}(i = 30^\circ, \text{e} = 0^\circ, \phi = 0^\circ, \lambda) * B, \quad (4)$$

where B is a constant that normalizes the RELAB *REFF*, $REFF^{RELAB}_{Spectralon}(i = 30^\circ,\ e = 0^\circ,\ \phi = 0^\circ,\ \lambda)$, to MISR's *REFF*, $REFF^{MISR}_{Spectralon}(i, e = 0^\circ, \phi = 0^\circ, \lambda)$, for example, at $i = 8^\circ$ and $B = REFF^{MISR}_{Spectralon}(i = 8^\circ, e = 0^\circ, \phi = 0^\circ, 633\ \text{nm})/REFF^{RELAB}_{Spectralon}(i = 30^\circ, e = 0^\circ, \phi = 0^\circ, 633\ \text{nm})$.

Figure 11 shows the comparisons of the $REFF_{Spectralon}$ of this work and that of the MISR at 633 nm. For incident zenith angles 8°, 40°, and 45°, the differences between our data and MISR increase as the viewing zenith angle becomes larger. The maximum difference is less than 5% for viewing zenith angles smaller than 60°. For incident angles 50° and 55°, the maximum differences are less than 3%. The comparisons and differences can be better perceived in the principal plane data plot shown in Fig. 12. Due to the rough nature (shown in Fig. 13) of the Spectralon surface, an up to 2% REFF variation exists when the Spectralon is aligned along different directions (McGuckin *et al.*, 1997). The error increases for large zenith angles due to the lower collection efficiency.

We also compared the Spectralon *REFF* data measured by the spectro-goniometer and our lab's three-color goniometer that is capable of measuring the *REFF* of particular surfaces in three wavelengths (473, 532, and 633 nm) at the various incident and view zenith angles in the principal plane (https://psi.cug.edu.cn/sysjs/gxsys.htm) (Zhang *et al.*, 2014 and Jiang *et al.*, 2019). Since both the three-color goniometer and the spectro-goniometer use identical sample holders, a cross-comparison of measurements made on the same samples by both instruments can further validate the performance of the spectro-goniometer. We selected two test samples, the Spectralon and Orbitech's JSC-1A Martian Soil Simulant (MSS, see Sec. IV below) (McKay *et al.*, 1994; Allen *et al.*, 1998; and Sibille *et al.*, 2006), and made measurements using the two instruments at three typical incident zenith angles, i = 8°, 45°, and 55°. For each sample measured at each incident zenith angle, four measurements were made, and the sample surface was rotated 90° between the adjacent measurement to estimate the influence of surface heterogeneities. The comparison results shown in Fig. 14 indicate that data measured by the two instruments agree with each other very well except for

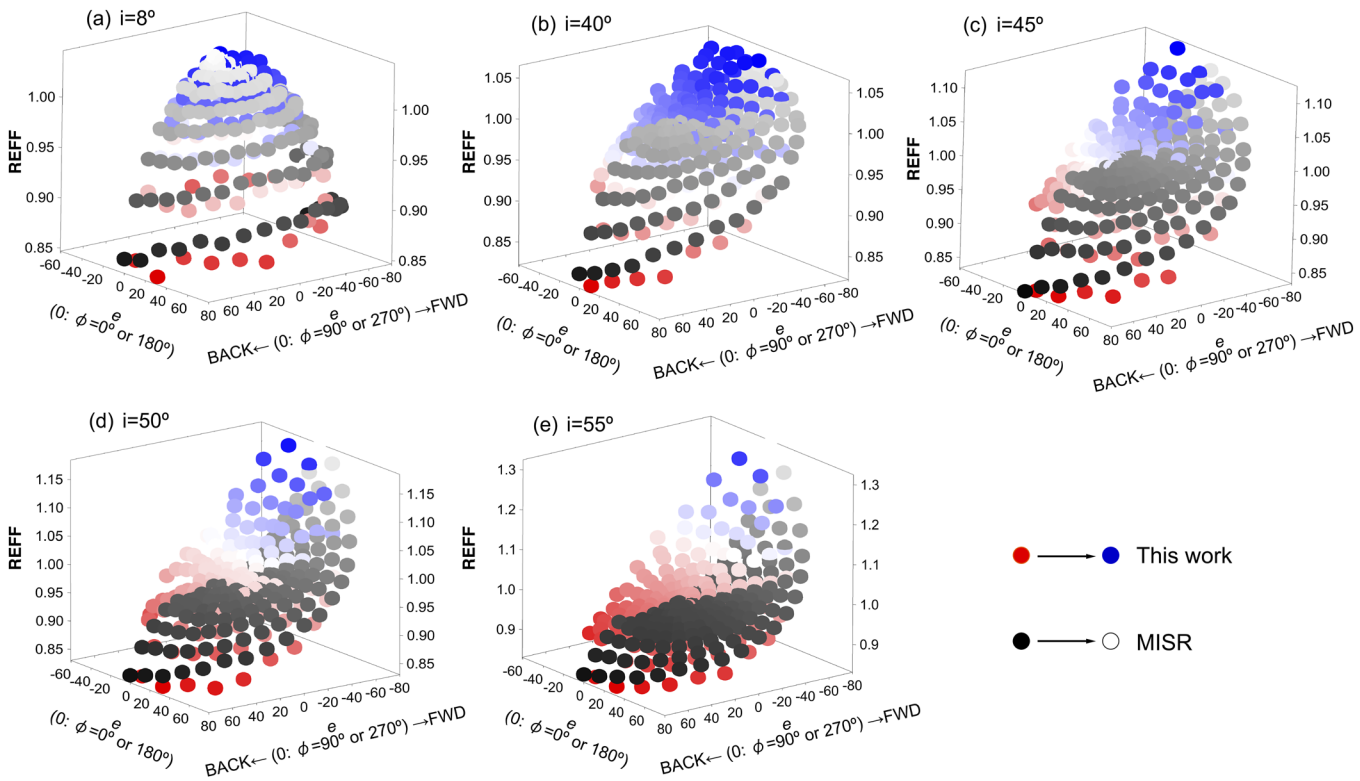

FIG. 11. Comparison of the 633 nm Spectralon *REFF* measured in this work (circles with color from red to blue) and that of the MISR measurement (circles with color from black to white) (McGuckin *et al.*, 1996; 1997; and Bruegge *et al.*, 2001): (a) i = 8°, (b) i = 40°, (c) i = 45°, (d) i = 50°, and (e) i = 55°. Both the x and y axes are viewing zenith angles e and BACK and FWD stand for backward and forward directions, respectively.

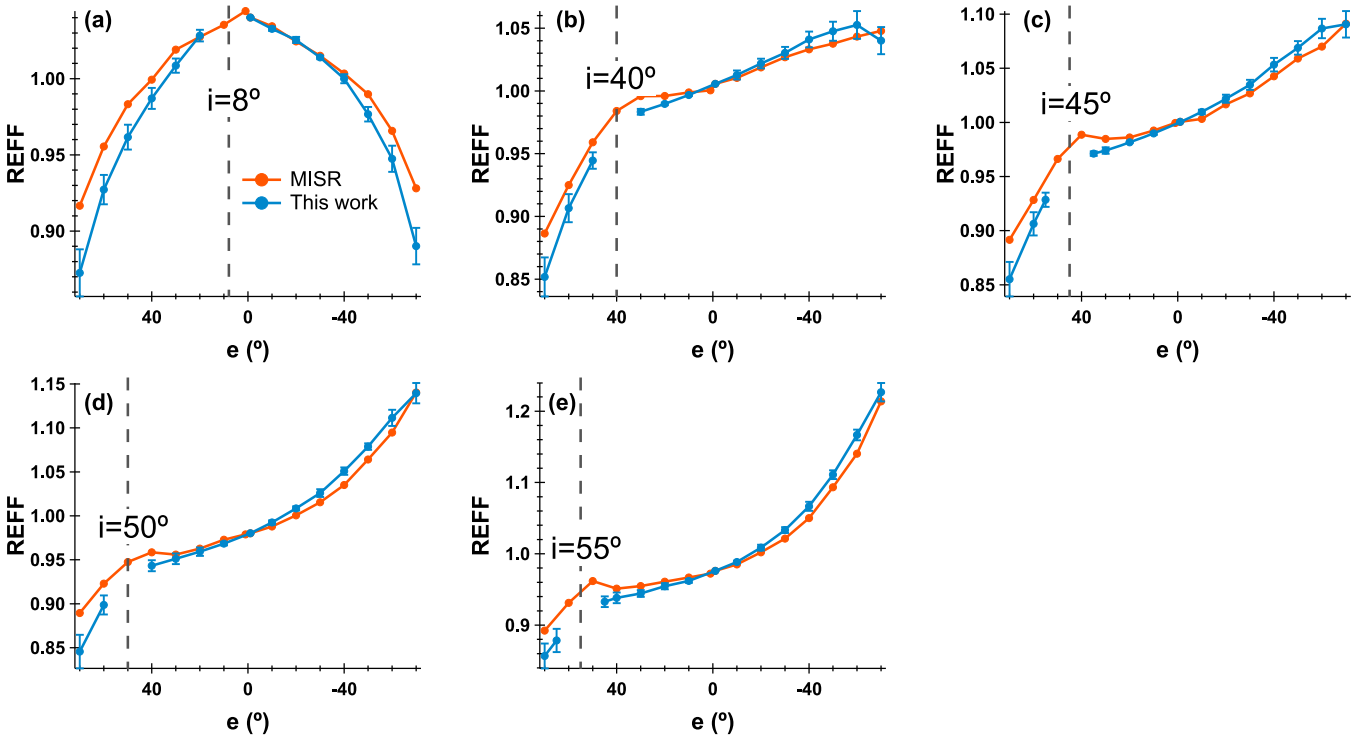

FIG. 12. Comparison of the 633 nm Spectralon *REFF* measured in the principal plane measured in this work and by MISR (McGuckin *et al.*, 1996; 1997; and Bruegge *et al.*, 2001): (a) $i = 8°$, (b) $i = 40°$, (c) $i = 45°$, (d) $i = 50°$, and (e) $i = 55°$. In each plot, the blue curve is the average of four measurements and the error bars represent one standard deviation. The Spectralon surface was rotated ~90° around the central vertical axis between measurements.

the JSC-1A at $i = 8°$ illumination that a maximum of ~6% difference in *REFF* exists, possibly due to the sample surface settle down when transferring the sample between the instruments. The influence of surface heterogeneity is minor, typically within 3% in *REFF* values, and slightly increases at very large view zenith angles.

E. Effects of surface tilting and height variation

We have studied the effects of surface tilt and surface height variations using measurements on Spectralon at $i = 45°$ in the principal plane. The positive and negative tilt angles correspond to the counter-clockwise and clockwise rolls of the surface when the observer is facing the sample [Fig. 15(a)]. As shown in Fig. 15, a positive increase of the tilt angle will make the surface more forward scattering and less backscattering. A similar effect occurs when the Spectralon surface is lower than the correct level, but the REFF changes are relatively smaller. These results indicate that the accurate alignment of the sample surface is more critical than surface height in measuring the correct angular scattering behavior of a flat sample.

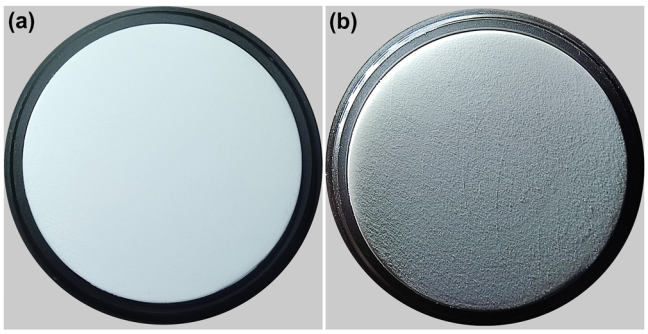

FIG. 13. The Spectralon illuminated from directly above the surface (a) and from the upper left (b). The viewing direction is the same as above.

F. Measurements on planetary analog materials

In this section, we present the spectral and photometric measurement results of two widely used planetary analog materials, the OrbiTech JSC-1A Lunar Regolith Simulant (LRS) and the JSC-1A MSS. Figure 16 shows the *REFF* spectra at different viewing zenith angles in the principal plane at two typical incident zenith angles, 8° and 45°. One can see from this plot that both the visual appearance and the reflectance spectra show the JSC-1A MSS is brighter and redder than the JSC-1A LRS in the visible. For both samples, their reflectance spectra measured at different viewing positions show larger spreads in relative reflectance values and spectral slopes at large ($i = 45°$) incident angle. Figures 16(e) and 16(f) show that, for the JSC-1A MSS, multiple measurements have reduced the noise level in the NIR region to better than 3% for $i = 8°$ and $i = 45°$.

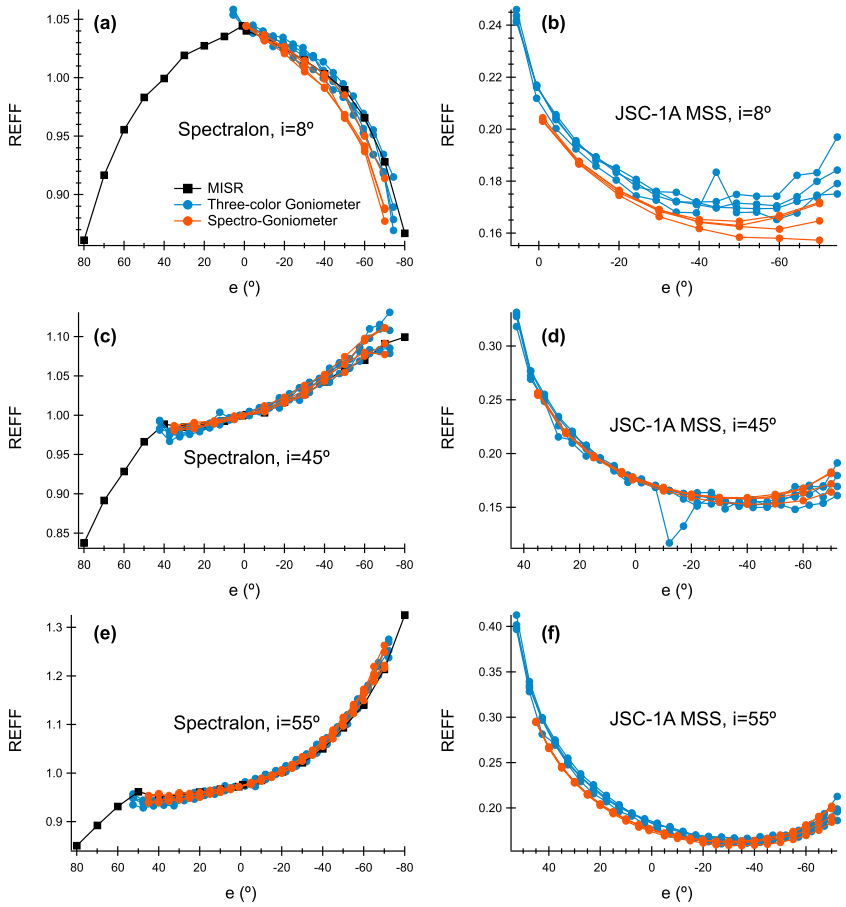

FIG. 14. *REFF* of the Spectralon [(a), (c), and (e)] and the JSC-1A Martian soil simulant [(b), (d), and (f)] measured by the three-color goniometer and this spectro-goniometer in 633 nm. The MISR Spectralon data are also included for comparisons.

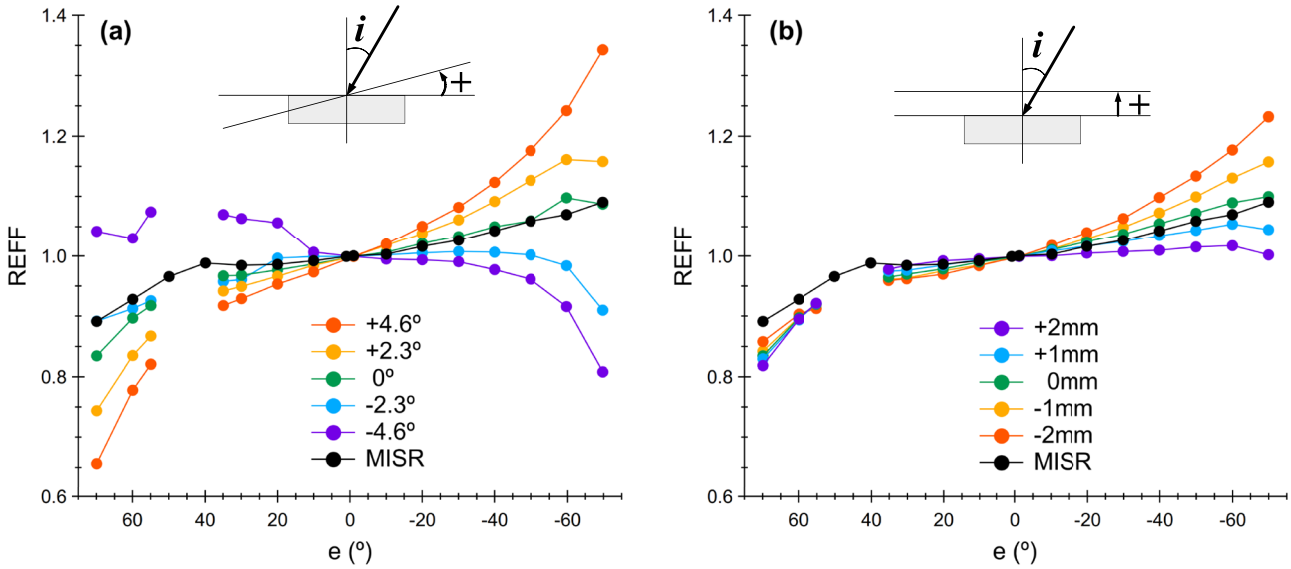

FIG. 15. Effects of sample surface tilting (a) and surface height variations (b) on measured Spectralon REFF at $i = 45°$ in the principal plane. The definitions of positive tilt angle and height change are indicated.

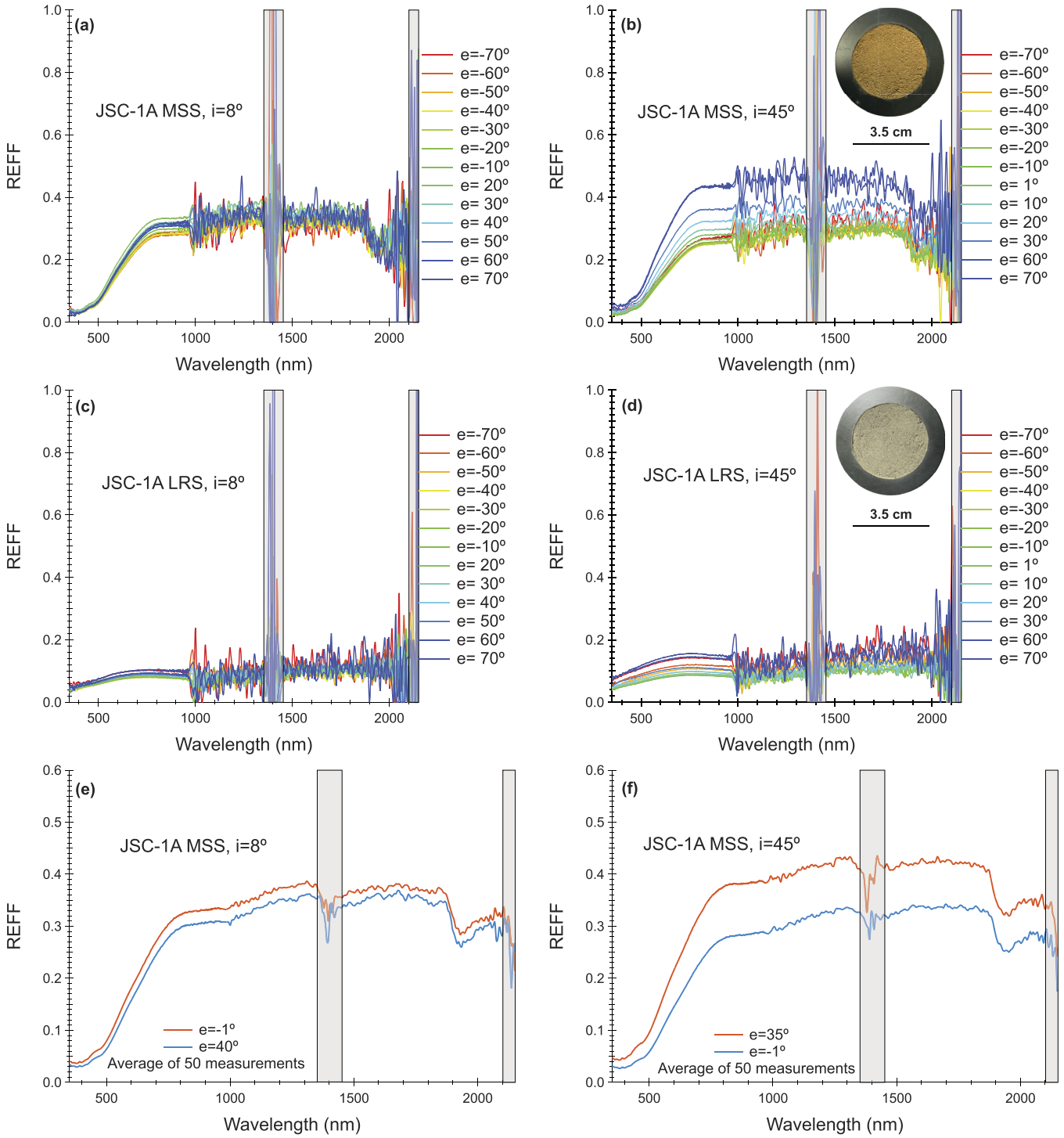

FIG. 16. Reflectance spectra of the JSC-1A Martian Soil Simulant (JSC-1A MSS) and the JSC-1A Lunar Regolith Simulant (JSC-1A LRS) measured at incident zenith angles of 8° and 45°. (a) i = 8° and (b) i = 45° for the JSC-1A MSS; (c) i = 8° and (d) i = 45° for the JSC-1A LRS. For clarity, only spectra measured in the principal plane are shown. (e) and (f) show how multiple measurements can reduce the noise level using the JSC-1A MSS as an example. Positive and negative viewing zenith angles correspond to measurement positions with 0° and 180° relative azimuth angles, respectively. Gray boxes indicate regions with low SNR values.

We also present the *REFF* at 633 nm and color ratios of 800 and 500 nm, *REFF*(800 nm)/*REFF*(500 nm), as typical measurement data. The color ratio can characterize the spectral shape and absorption features at different scattering configurations and is an important signature of multiple scattering contribution for many planetary surfaces (e.g., Adams and Filice, 1967; Veverka *et al.*, 1978a; 1978b; Abe *et al.*, 2006; and Hapke, 2012).

Figures 17 and 18 show the *REFF* in contour plot and the color ratio *REFF*(800 nm)/*REFF*(500 nm) for the two samples, respectively. In each contour plot, the center point corresponds to the nadir ($e = 0°$), the radius from the center measures zenith angles (either incident or viewing), and the azimuth angle measured from due north (the incident direction) is the relative azimuth angle ϕ (from 0° to 360° counter-clockwise). In addition, the incident

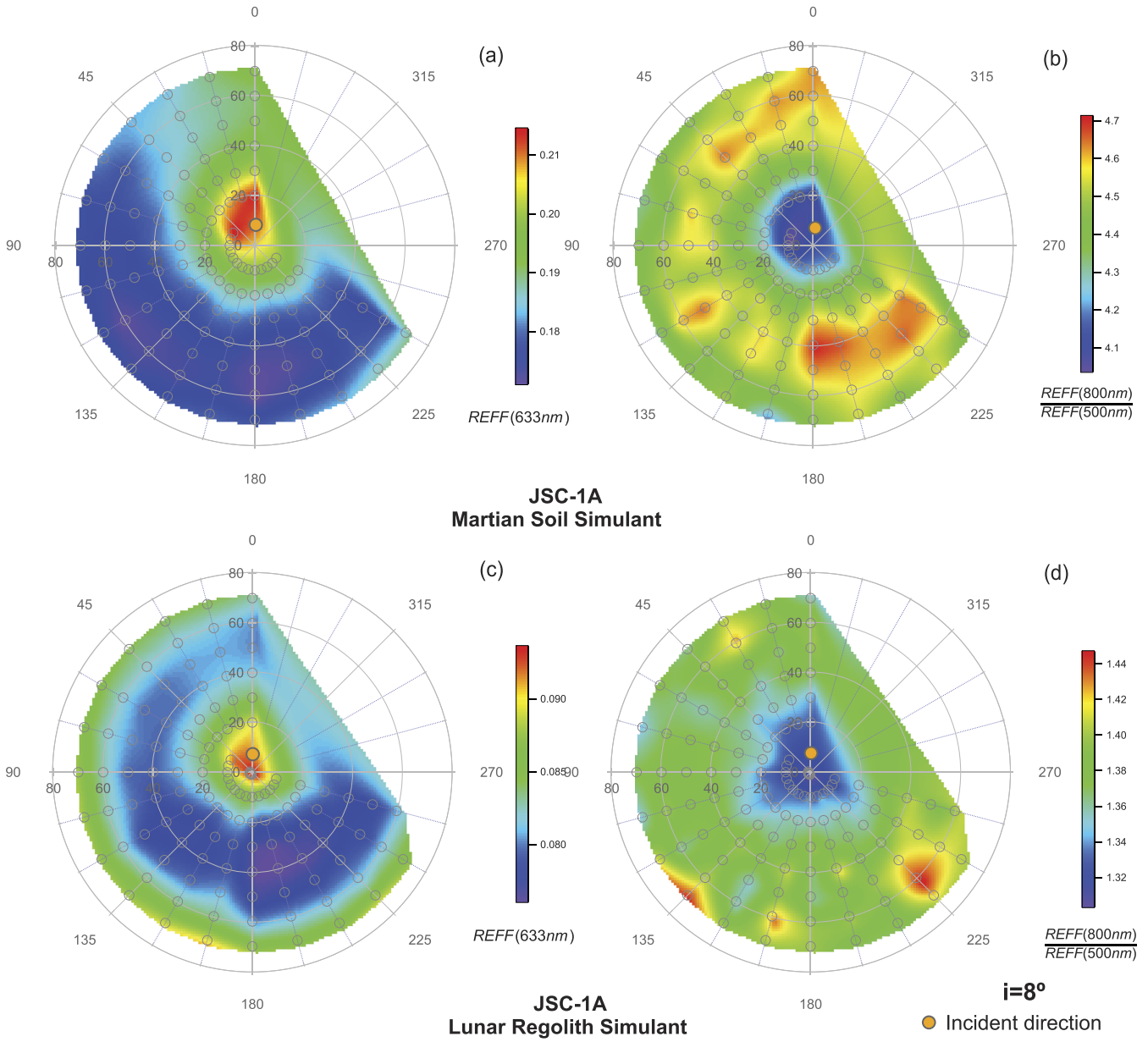

FIG. 17. *REFF* (633 nm) and color ratio [*REFF* (800 nm)/*REFF* (500 nm)] of the JSC-1A MSS and the JSC-1A LRS in the upper hemisphere for $i = 8°$. (a) *REFF* in 633 nm for the JSC-1A MSS, (b) [*REFF* (800 nm)/*REFF* (500 nm)] for the JSC-1A MSS, (c) *REFF* in 633 nm for the JSC-1A MSS, and (d) [*REFF* (800 nm)/*REFF* (500 nm)] for the JSC-1A LRS. The solid orange circle in each plot indicates the incident direction, and the hollow gray circles indicate the discrete viewing positions. Colored dots (too dense to be distinguishable) are interpolations of the measurement data.

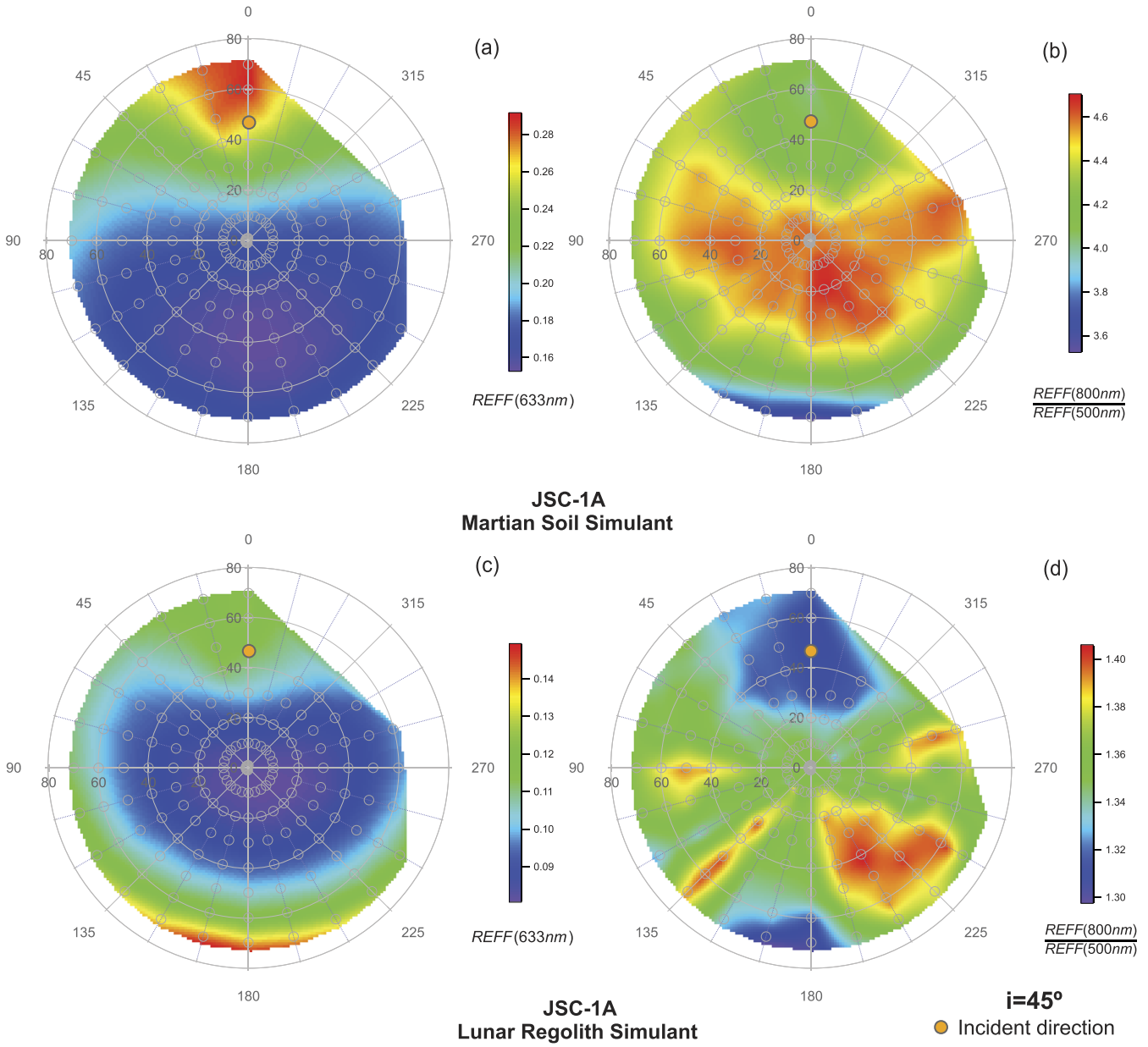

FIG. 18. *REFF* (633 nm) and color ratio [*REFF* (800 nm)/*REFF* (500 nm)] of the JSC-1A MSS and the JSC-1A LRS in the upper hemisphere for $i = 45°$. (a) *REFF* in 633 nm for the JSC-1A MSS, (b) [*REFF* (800 nm)/*REFF* (500 nm)] for the JSC-1A MSS, (c) *REFF* in 633 nm for the JSC-1A MSS, and (d) [*REFF* (800 nm)/*REFF* (500 nm)] for the JSC-1A LRS. The solid orange circle in each plot indicates the incident direction, and the hollow gray circles indicate the discrete viewing positions. Colored dots (too dense to be distinguishable) are interpolations of the measurement data.

direction is indicated by an orange circle and the measurement positions are marked by gray circles. Discrete data points were interpolated using Voronoi polygons to generate *REFF* values at denser non-measurement positions with a ~1° step.

At incident angle 8°, the JSC-1A MSS is strongly backscattering [Fig. 17(a)] while the JSC-1A LRS shows both back- and forward-scattering lobes [Fig. 17(c)]. As the phase angle α (the angle between the incident and the viewing directions) increases, the color ratio *REFF* (800 nm)/*REFF* (500 nm) of the JSC-1A MSS first increases and then decreases after reaching the maximum value around $\alpha = 50°$ [Fig. 17(b)]. In contrast, the color ratio of the JSC-1A LRS increases and then levels off [Fig. 17(d)].

At 45° incident zenith angle, the JSC-1A MSS is still strongly backscattering [Fig. 18(a)] while the JSC-1A LRS becomes strongly

forward-scattering [Fig. 18(c)]. The color ratios of both samples increase and then decrease as the phase angle increases.

These trends generally resemble previous laboratory measurements on Martian and Lunar analog materials (e.g., Johnson *et al.*, 2013; Pommerol *et al.*, 2013; and Schröder *et al.*, 2014). Compared with the *in situ* measurement on the lunar surface (e.g., Jin *et al.*, 2015 and Jiang *et al.*, 2021), the JSC-1A LRS shows less pronounced backscattering, stronger forward scattering, and a smaller phase angle where the color ratio transited from reddening to bluing. These differences should be the results of differences in composition, physical property, and measurement geometry. For instance, Schröder *et al.*, (2014) suggested that the maximum color ratio appears at larger phase angles for the large incident angle, which is the case for Chang'E-3 and Chang'E-4 with $i \approx 80^\circ$ (Jin *et al.*, 2015 and Jiang *et al.*, 2021). In general, the measurement results of MSS show red-shaped spectra and a strong phase reddening effect, similar to those *in situ* measurements (e.g., Guinness 1981; Johnson *et al.*, 2006a; 2006b; 2015; and 2021). Due to the much greater diversity of Martian surface materials, it is normal that laboratory measurements show some subtle differences, for example, the absolute values of the reflectance.

IV. CONCLUSIONS

We have described a simple spectro-goniometric system that can measure the bi-directional reflectance of particulate samples in the wavelength range from 350 to 2150 nm. The use of optic fibers to transmit the incident and the scattered light allows an easy and flexible scheme for achieving the desired incident and viewing angular positions. Although the fiber absorptions in the short-wave infrared region (960–2150 nm) have led to higher noise, the signal-to-noise ratio can be improved by performing multiple measurements. The system has a very high signal-to-noise ratio in the short wavelength region and a very good linearity response. Comparisons of measurements on Labsphere Spectralon with published data and with our three-color goniometer indicate that the system has correct photometric behavior. We also presented its first measurements on typical planetary analog material, JSC-1A Lunar regolith and Martian soil simulants, for future cross laboratory comparisons. Although the goniometric part of the system is not motorized, its construction is very simple and cost-effective, and the manual operation can easily avoid any potential fiber entanglement hazards. More measurements will be applied to a wider material range for remote sensing.

Currently, the smallest phase angle achievable is 10° due to the large size of the lens used in the incident optics assembly. The minimum phase angle can be pushed down to 3°–5° by increasing the distance between the sample surface and both the incident and the collection optics assemblies but at the cost of deteriorated SNR. Future efforts will be made to increase the incident irradiance by using a light source with higher output power and optic fibers with higher transmittance, so the backscattering region can be measured with sufficient SNR.

ACKNOWLEDGMENTS

The authors thank two anonymous reviewers for their useful comments that improved the quality of this paper. This work was supported by the National Natural Science Foundation of China (Grant Nos. 12073024, 11773023, and 11941001) and the Civil Aerospace Pre-research Project (No. D020302).

AUTHOR DECLARATIONS

Conflict of Interest

All authors declare that they have no conflicts of interest.

DATA AVAILABILITY

The data that support the findings of this study are available from the corresponding author upon reasonable request.

REFERENCES

Abe, M., Takagi, Y., Kitazato, K., Abe, S., Hiroi, T., Vilas, F. *et al.*, "Near-infrared spectral results of asteroid Itokawa from the Hayabusa spacecraft," Science **312**(5778), 1334–1338 (2006).

Adams, J. B. and Filice, A. L., "Spectral reflectance 0.4 to 2.0 microns of silicate rock powders," J. Geophys. Res. **72**(22), 5705–5715, https://doi.org/10.1029/JZ072i022p05705 (1967).

Allen, C. C., Jager, K. M., Morris, R. V., Lindstrom, D. J., Lindstrom, M. M., and Lockwood, J. P., "Martian soil simulant available for scientific, educational study," EOS **79**, 405–409 (1998).

Bruegge, C., Chrien, N., and Haner, D., "A Spectralon BRF data base for MISR calibration applications," Remote Sens. Environ. **77**(3), 354–366 (2001).

Bhandari, A., Hamre, B., Frette, Ø., Zhao, L., Stamnes, J. J., and Kildemo, M., "Bidirectional reflectance distribution function of Spectralon white reflectance standard illuminated by incoherent unpolarized and plane-polarized light," Appl. Opt. **50**(16), 2431 (2011).

Clark, B. E., Helfenstein, P., Bell, J. F., Peterson, C., Veverka, J., Izenberg, N. I. *et al.*, "NEAR infrared spectrometer photometry of asteroid 433 Eros," Icarus **155**(1), 189–204 (2002).

Gehrels, T., Coffeen, T., and Owings, D., "Wavelength dependence of polarization. III. The lunar surface," Astron. J. **69**, 826 (1964).

Guinness, E. A., "Spectral properties (0.40 to 0.75 microns) of soils exposed at the Viking 1 landing site," J. Geophys. Res.: Solid Earth **86**(B9), 7983–7992, https://doi.org/10.1029/JB086iB09p07983 (1981).

Gunderson, K., Lüthi, B., Russell, P., and Thomas, N., "Visible/NIR photometric signatures of liquid water in Martian regolith simulant," Planet. Space Sci. **55**(10), 1272–1282 (2007).

Gunderson, K., Thomas, N., and Whitby, J. A., "First measurements with the Physikalisches Institut Radiometric Experiment (PHIRE)," Planet. Space Sci. **54**(11), 1046–1056 (2006).

Hapke, B., *Theory of Reflectance and Emittance Spectroscopy*, 2nd ed. (Cambridge University Press, 2012).

Jiang, T., Hu, X., Zhang, H., Ma, P., Li, C., Ren, X. *et al.*, "In situ lunar phase curves measured by Chang'E-4 in the Von Kármán Crater, South Pole-Aitken basin," Astron. Astrophys. **646**, A2 (2021).

Jiang, T., Zhang, H., Yang, Y., Hu, X., Ma, P., Sun, Y. *et al.*, "Bi-directional reflectance and polarization measurements of pulse-laser irradiated airless body analog materials," Icarus **331**, 127–147 (2019).

Jin, W., Zhang, H., Yuan, Y., Yang, Y., Shkuratov, Y. G., Lucey, P. G. *et al.*, "In situ optical measurements of Chang'E-3 landing site in Mare Imbrium: 2. Photometric properties of the regolith," Geophys. Res. Lett. **42**(20), 8312–8319, https://doi.org/10.1002/2015GL065789 (2015).

Johnson, J. R., Grundy, W. M., Lemmon, M. T., Bell, J. F., Johnson, M. J., Deen, R. G. *et al.*, "Spectrophotometric properties of materials observed by Pancam on the Mars Exploration Rovers: 1. Spirit," J. Geophys. Res.: Planets **111**(E2), S14, https://doi.org/10.1029/2005JE002494 (2006a).

Johnson, J. R., Grundy, W. M., Lemmon, M. T., Bell, J. F., Johnson, M. J., Deen, R. *et al.*, "Spectrophotometric properties of materials observed by Pancam on the Mars Exploration Rovers: 2. Opportunity," J. Geophys. Res.: Planets **111**(E12), S16, https://doi.org/10.1029/2006JE002762 (2006b).

Johnson, J. R., Shepard, M. K., Grundy, W. M., Paige, D. A., and Foote, E. J., "Spectrogoniometry and modeling of Martian and lunar analog samples and Apollo soils," Icarus **223**(1), 383–406 (2013).

Johnson, J. R., Grundy, W. M., Lemmon, M. T., Bell, J. F., and Deen, R. G., "Spectrophotometric properties of materials observed by Pancam on the Mars Exploration Rovers: 3. Sols 500–1525," Icarus **248**, 25–71 (2015).

Johnson, J. R., Grundy, W. M., Lemmon, M. T., Liang, W., Bell, J. F., Hayes, A. G., and Deen, R. G., "Spectrophotometric properties of materials observed by Pancam on the Mars Exploration Rovers: 4. Final mission observations," Icarus **357**, 114261 (2021).

McGuckin, B. T., Haner, D. A., Menzies, R. T., Esproles, C., and Brothers, A. M., "Directional reflectance characterization facility and measurement methodology," Appl. Opt. **35**(24), 4827 (1996).

McGuckin, B. T., Haner, D. A., and Menzies, R. T., "Multiangle imaging spectroradiometer: Optical characterization of the calibration panels," Appl. Opt. **36**(27), 7016–7022 (1997).

McKay, D. S. *et al.*, "JSC-1: A new lunar soil simulant," in *Engineering, Construction, and Operations in Space IV* (American Society of Civil Engineers, 1994), Vol. 2, pp. 857–866.

Pieters, C. M. and Hiroi, T., "RELAB (Reflectance Experiment Laboratory): A NASA multiuser spectroscopy facility," in 35th Lunar and Planetary Science Conference. No. 1720 (2004).

Pommerol, A., Thomas, N., Jost, B., Beck, P., Okubo, C., and McEwen, A.S., "Photometric properties of Mars soils analogs," J. Geophys. Res.: Planets **118**, 2045 (2013).

Pommerol, A., Jost, B., Poch, O., Yoldi, Z., Brouet, Y., Gracia-Berná, A. *et al.*, "Experimenting with mixtures of water ice and dust as analogues for icy planetary material: Recipes from the Ice Laboratory at the University of Bern," Space Sci. Rev. **215**(5), 37 (2019).

Shepard, M. K., "The Bloomsburg University Goniometer (B. U. G.) Laboratory: An integrated laboratory for measuring bidirectional reflectance functions," in 32nd Lunar and Planetary Science Conference No. 1015 (2001).

Shepard, M. K. and Helfenstein, P., "A test of the Hapke photometric model," J. Geophys. Res. **112**(E3), 001, https://doi.org/10.1029/2005JE002625 (2007).

Shkuratov, Y., Bondarenko, S., Kaydash, V., Videen, G., Muñoz, O., and Volten, H., "Photometry and polarimetry of particulate surfaces and aerosol particles over a wide range of phase angles," J. Quant. Spectrosc. Radiat. Transfer **106**(1–3), 487–508 (2007).

Sibille, L. *et al.*, "Lunar regolith simulant materials: Recommendations for standardization, production, and usage," NASA Technical Report No. 2006-214605, 2006.

Schröder, S. E., Grynko, Y., Pommerol, A., Keller, H. U., Thomas, N., and Roush, T. L., "Laboratory observations and simulations of phase reddening," Icarus **239**, 201–216 (2014).

Sun, Z. Q., Wu, Z. F., and Zhao, Y. S., "Semi-automatic laboratory goniospectrometer system for performing multi-angular reflectance and polarization measurements for natural surfaces," Rev. Sci. Instrum. **85**(1), 014503 (2014).

Svensen, Ø., Kildemo, M., Maria, J., Stamnes, J. J., and Frette, Ø., "Mueller matrix measurements and modeling pertaining to Spectralon white reflectance standards," Opt. Express **20**(14), 015045 (2012).

Veverka, J., Goguen, J., Yang, S., and Elliot, J. L., "Near-opposition limb darkening of solids of planetary interest," Icarus **33**(2), 368–379 (1978a).

Veverka, J., Goguen, J., Yang, S., and Elliot, J., "Scattering of light from particulate surfaces," Icarus **34**(2), 406–414 (1978b).

Voss, K. J., Chapin, A., Monti, M., and Zhang H., "Instrument to measure the bidirectional reflectance distribution function of surfaces," Appl. Opt. **39**, 6197–6206 (2000).

Voss, K. J. and Zhang, H., "Bidirectional reflectance of dry and submerged Labsphere Spectralon plaque," Appl. Opt. **45**, 7924–7927 (2006).

Yang, Y. Z., Li, S., Milliken, R. E., Zhang, H., Robertson, K., and Hiroi, T., "Phase functions of typical lunar surface minerals derived for the Hapke model and implications for visible to near-infrared spectral unmixing," J. Geophys. Res.: Planets **124**, 31–60, https://doi.org/10.1029/2018JE005713 (2019).

Zhang, H. and Voss, K. J., "Comparisons of bidirectional reflectance distribution function measurements on prepared particulate surfaces and radiative-transfer models," Appl. Opt. **44**, 597 (2005).

Zhang, H. and Voss, K. J., "Bi-directional reflectance measurement of closely packed natural and prepared particulate layers," in *Light Scattering Reviews III*, edited by A. Kokhanovsky (Springer, 2008).

Zhang, H., Jin, W., Xu, W., Wang, Z., and Sun, H., "A goniometric system to measure the incomplete Mueller matrices of packed layers," in 45th Lunar and Planetary Science Conference, 2014.